Electronic Supplementary Material (ESI) for Physical Chemistry Chemical Physics.

Supporting Information: Thermodynamic stability of Li-B-C compounds from first principles.

Saba Kharabadze,[1] Maxwell Meyers,[1] Charlsey R. Tomassetti,[1]
Elena R. Margine,[1] Igor I. Mazin,[2] and Aleksey N. Kolmogorov[1]

[1] *Department of Physics, Applied Physics and Astronomy, Binghamton University, State University of New York, PO Box 6000, Binghamton, New York 13902-6000, USA.*

[2] *Department of Physics and Astronomy, George Mason University, Fairfax, Virginia 22030, USA and Quantum Science and Engineering Center, George Mason University, Fairfax, Virginia 22030, USA*

(Dated: February 7, 2023)

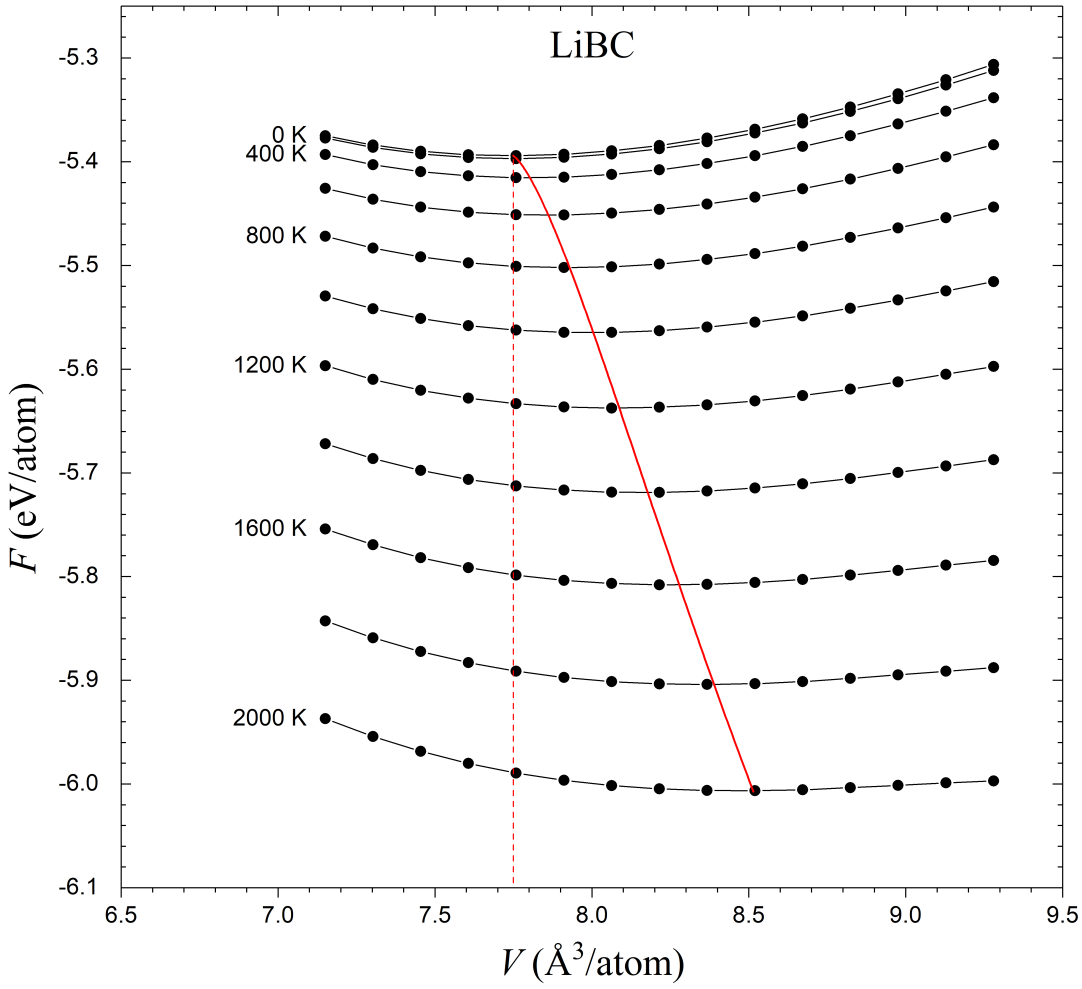

Figure S1. Quasi-harmonic approximation (QHA) results for LiBC. In these simulations, we (i) generated a uniform grid of volumes around equilibrium by rescaling the lattice constants; (ii) optimized the unit cell shape and atomic positions at each fixed volume with VASP; (iii) used Phonopy and VASP to perform phonon calculations in the harmonic approximation at each volume; (iv) fitted the resulting free energy points at each temperature with a third-order polynomial; and (v) showed the free energy values for every 200 K (black circles), the polynomial fits (black solid lines), the minimum free energy values at the corresponding volumes for every 10 K (red solid line), and the starting volume (red dashed line). At 1800 K, the free energy difference between the standard harmonic formalism and the QHA values was found to be 21.53 meV/atom.

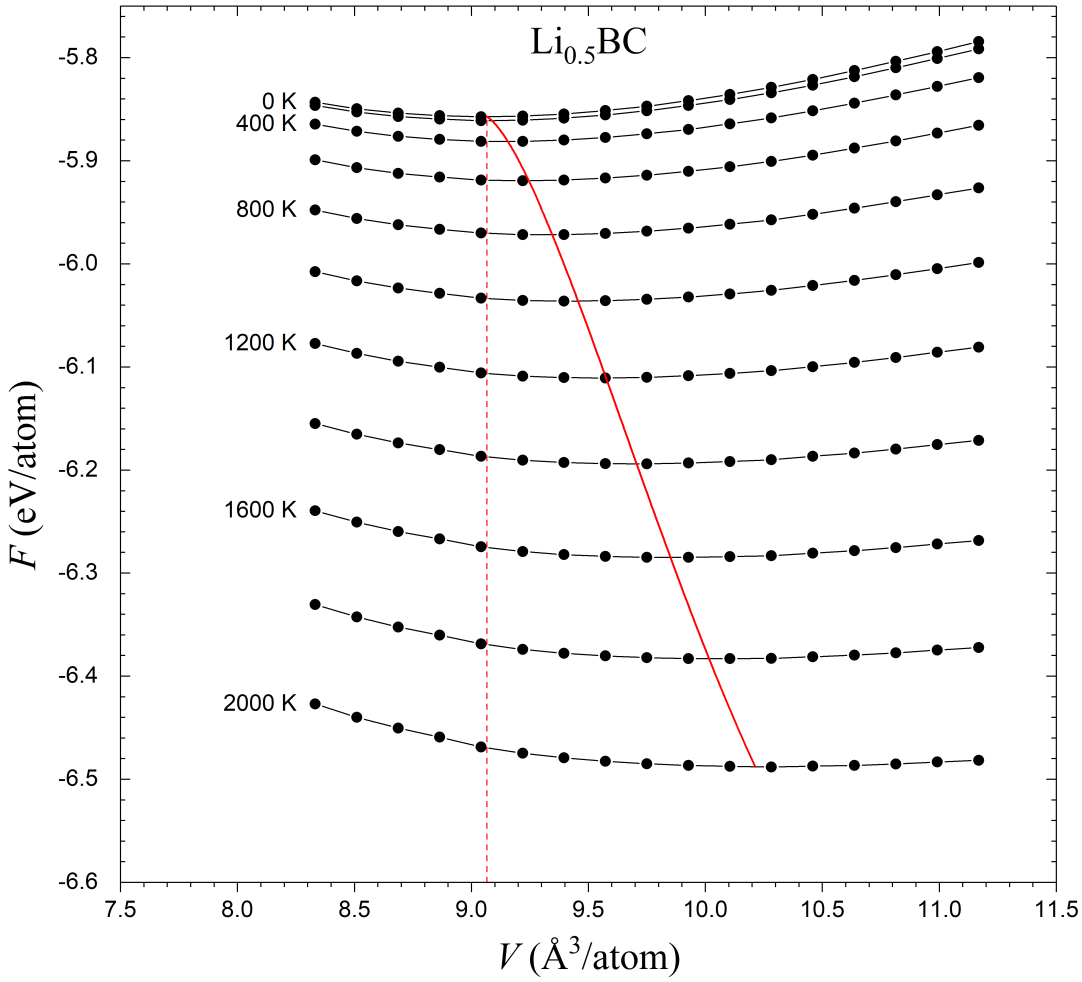

Figure S2. QHA results for $Li_{0.5}BC$. The simulation and analysis procedure is described in Figure S3. At 1800 K, the free energy difference between the standard harmonic formalism and the QHA values was found to be 23.16 meV/atom. These LiBC and $Li_{0.5}BC$ results were used to assess the significance of the anharmonic effect on the Gibbs free energy difference defining the phase boundary between $Li_2B_2C_2$ and $1/2Li_2$+LiB_2C_2 in Fig. 4(a). The volume expansion in the solid phases change the Gibbs free energy difference by $6 \times (-21.53$ meV/atom$) - 5 \times (-23.16$ meV/atom$) \approx -13.4$ meV/Li.

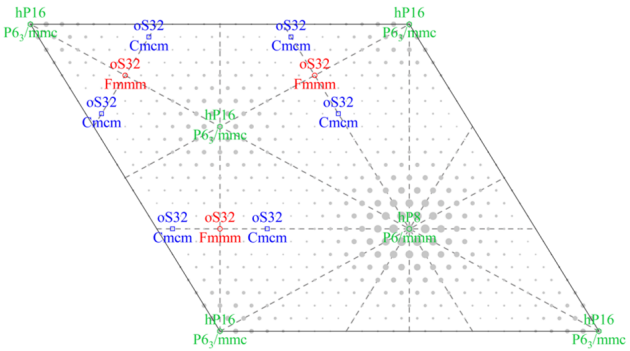

(*a*) Displacement map in g-BC_3

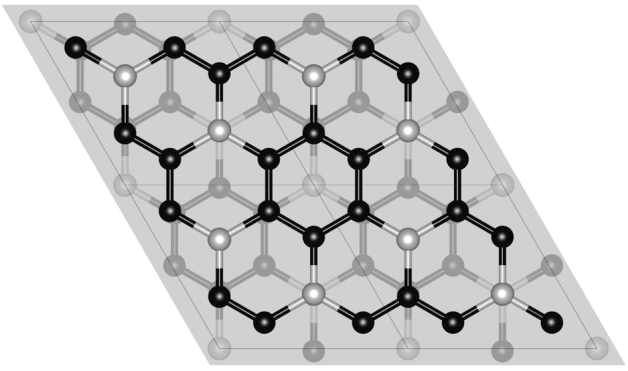

(*b*) g-BC_3 (hP16, P6$_3$/mmc)

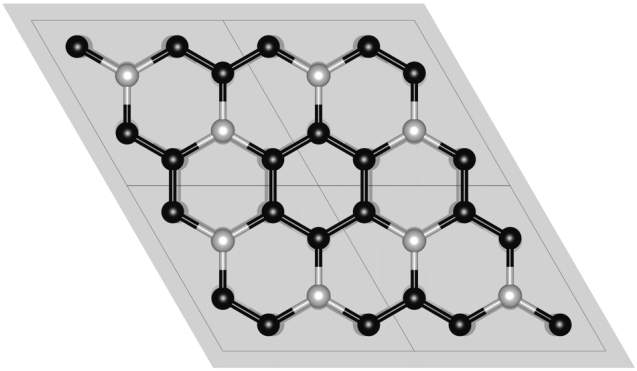

(*c*) e-BC_3 (oS32, Fmmm)

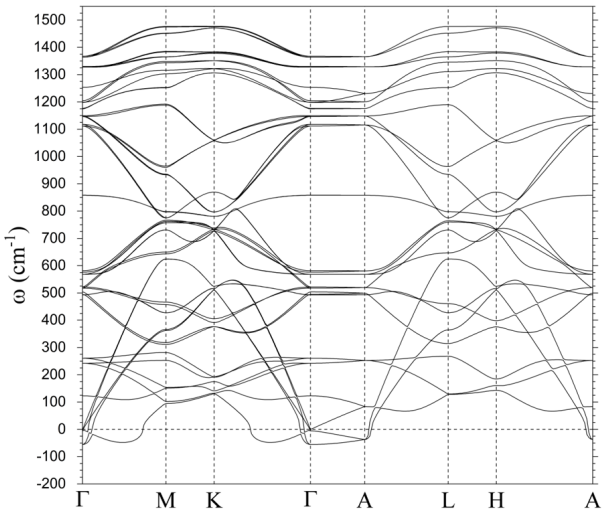

(*d*) Phonon dispersion in g-BC_3

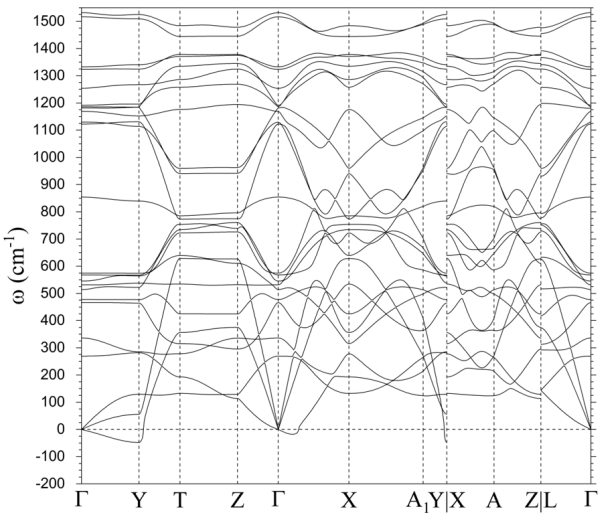

(*e*) Phonon dispersion in e-BC_3

Figure S3. Stability analysis of g-BC_3 and its derivatives. (a) A grid of examined displacements in g-BC_3. The location of each point on the grid corresponds to a rigid shift of one layer in the AB-stacked g-BC_3. Arbitrary shifts reduce the symmetry to mP16 (P2$_1$/m), shifts along the dotted lines result in oS32 (Cmcm), while shift to special points generate higher-symmetry orthorhombic or hexagonal unit cells. The size of each dot shows excess energy calculated without atomic or lattice constant optimizations. After optimization, the oS32 (Fmmm) configuration has the lowest energy, 15 meV/atom below that of g-BC_3. (b,c) Structures of g- and e-BC_3. (d,e) Phonon dispersions calculated in the harmonic approximation for g- and e-BC_3.

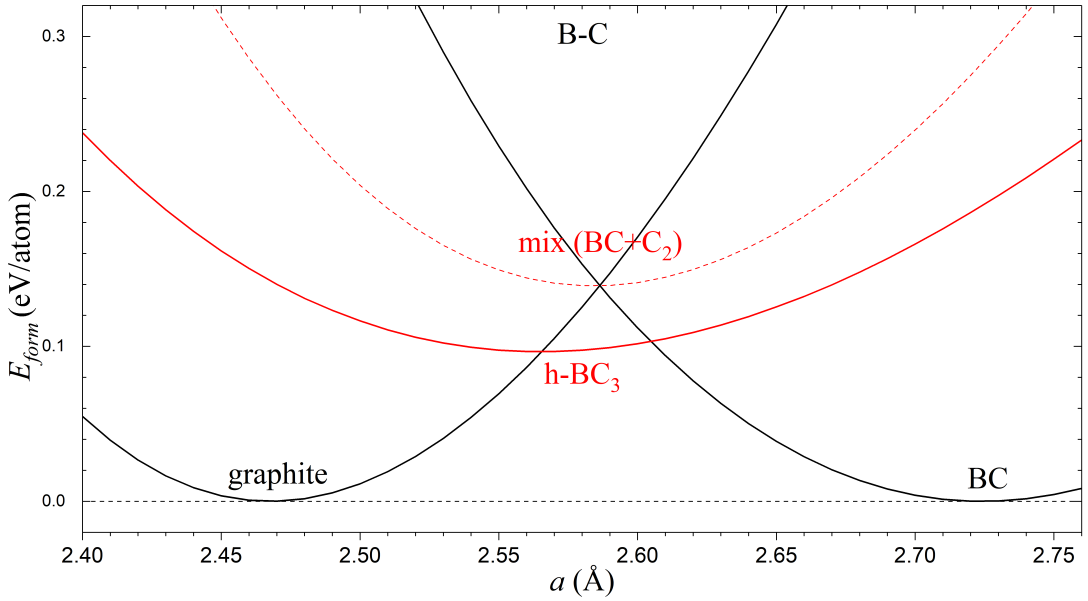

Figure S 4. Calculated equations of state for graphite, hypothetical BC, and reported h-BC_3 as a function of the in-plane lattice constants. The formation energies are referenced to the energies of graphite and BC at equilibrium. The dotted red line corresponds to the average energy of graphite and BC constrained to the same lattice constant value. The plot illustrates that the dominant part of the h-BC_3 positive formation energy results from the penalty associated with the C-C bond expansion and B-C bond compression.

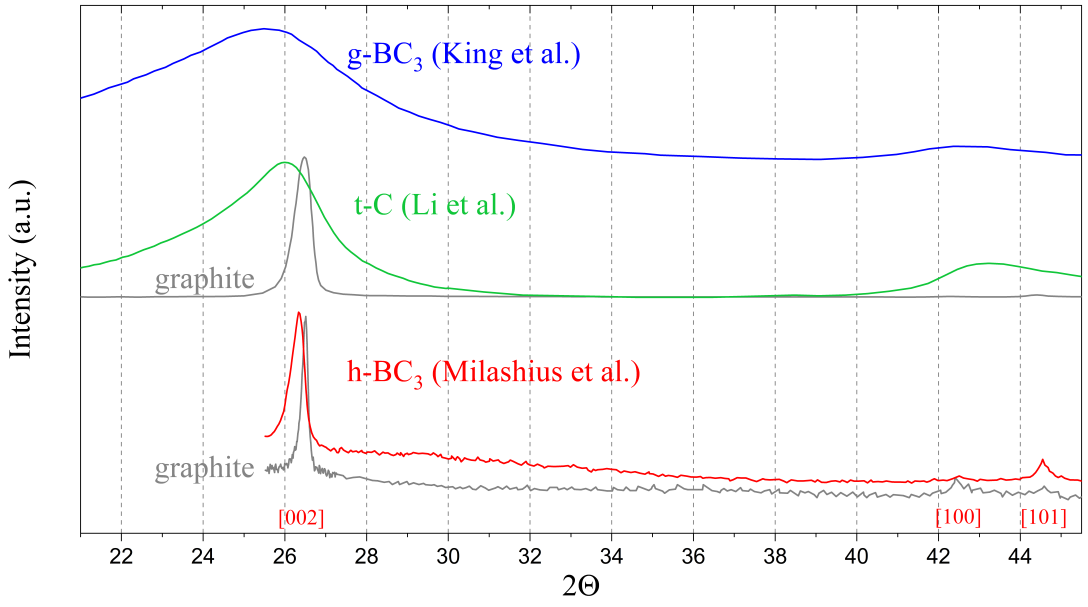

Figure S5. Comparison of powder XRD patterns adopted from experimental studies on precursor-based synthesis of g-BC_3 by King *et al.* [1], ball-milling preparation of turbostratic carbon by Li et al. [2], and direct synthesis of h-BC_3 by Milashius et al. [3]. The gray data sets correspond to the reported powder XRD patterns of graphite.

Phase name	Space group	Pearson symbol	$\Delta E_{\text{c. hull}}$ w/o ZPE	$\Delta E_{\text{c. hull}}$ w/ ZPE	$\Delta F_{\text{c. hull}}$ at 600 K	Lattice parameters (Å or °) a	b	c	α	β	γ	Ref.	Fig.
fcc-Li	$Fm\bar{3}m$	cF4	0	0	0.0004	4.318							1
bcc-Li	$Im\bar{3}m$	tI2	0.002	0.001	0	3.431							1
B	$R\bar{3}m$	hR36	0	0	0	4.901		12.540					1
C	P_3mmc	hP4	0	0	0	2.468		6.608					1
LiBC	$P6_3/mmc$	hP6	0	0	0	2.749		6.975					1
LiC_{12}	P6/mmm	hP13	0	0	0	4.299		6.936					1
LiC_6	P6/mmm	hP7	0	0	0	4.327		3.603					1
LiC	Immm	oI8	0	0	0	3.593	4.822	5.351					1
Li_4C_3	C2/m	mS14	0	0	0	6.566	3.797	6.220		118.05			1
Li_9B_8	$P6_3/mmc$	hP34	0	0	0	3.974		25.174					1
Li_8B_7	$P\bar{6}m2$	hP15	0	0	0.0009	3.973		11.035					1
LiB	$P6_3/mmc$	hP8	0.038	0.042	0.057	3.050		10.760					1
LiB_3	P4/mbm	tP16	0.009	0.008	0.006	5.966		4.148					1
Li_3B_{14}	$P\bar{4}$	tP136	0	0	0	10.768		8.768					1
B_4C	Cm	mS30	0	0	0	8.774	5.605	5.052		118.78			1, 6
$LiB_{13}C_2$	Imma	oI64	0	0	0	5.672	10.826	8.040					1
LiB_6C	Amm2	oS32	0	0	0	4.704	8.987	5.648					1
$B_{10.5}C^a$	P1	aP414	0			15.584	15.586	15.597	66.23	66.24	66.27	[4]	1, 6
$B_{6.67}C^a$	Cm	mS92	0			16.528	5.658	7.680		110.54		[4]	1, 6
g-BC_3	$P6_3/mmc$	hP16	0.232	*	*	5.173		6.896				[1][5]	5
e-BC_3	Fmmm	oS32	0.217	0.211*	0.202*	5.182	6.359	8.954					S3
r-BC_3	$P\bar{1}$	aP16	0.215	0.208*	0.199*	5.172	5.177	6.881	88.21	67.99	60.06		S3
a-BC_3	Pmma	oP8	0.196	0.183	0.190	2.509	2.514	7.815				[6]	5
b-BC_3	Pmma	oP8	0.204			2.485	2.523	7.900				[6]	5
c-BC_3	$I\bar{4}3m$	cI64	0.200	0.189	0.197	7.332						[7]	5
h-BC_3	$P\bar{6}m2$	hP4	0.431	*	*	2.565		6.717				[3]	5
h-BC_{3+x}	$P\bar{6}$	hP112	0.293			13.621		6.488					5
h-$LiBC_3$	$Pmn2_1$	oP10	0.223	*	*	2.618	7.481	4.406				[3]	8
g-$LiBC_3$	$Pmc2_1$	oP10	0.031	0.028	0.025	3.696	5.200	4.494					8
$Li_{0.5}BC$	Imm2	oI10	0.210	0.195	0.184	2.724	7.056	4.611					2
$Li_{0.5}BC$	$P\bar{3}1m$	hP15	0.225	0.209	0.197	4.687		7.043					2
$Li_{0.5}BC$	Pmma	oP10	0.221			7.027	2.712	4.679					2
$Li_{0.42}BC$	Pmm2	oP29	0.283			6.732	8.096	4.696					2
$Li_{0.5}BC$	P1	aP15	0.208			4.450	4.597	6.569	86.41	65.22	85.94		2
$Li_{0.67}BC$	$P\bar{6}2m$	hP8	0.118	0.109	0.104	4.704		3.540					
Li_2B_2C	$P\bar{4}m2$	tP10	0.772			4.139		7.106				[8]	9
$Li_2B_2C^b$	$P\bar{4}m2$	tP10	0.438	*	*	4.124		5.342					9
Li_2B_2C	$P4_2/mmc$	tP10	0.418			4.305		7.157					9
Li_2B_2C	Pm	mS20	0.190			4.256	10.647	4.190		117.77			9
Li_2B_2C	Cmcm	oS40	0.106			2.818	4.873	26.377					9

Table S1. Stability and lattice parameters of select Li-B-C phases obtained in our DFT calculations. References are given for phases most relevant to this study and full structural information is provided in CIF files. At $T = 0$ K, we constructed the full convex hull and indicated the distance to the convex hull ($\Delta E_{\text{c. hull}}$ in eV/atom). For key phases, we performed phonon calculations and showed the distance to the convex hull constructed at $T = 0$ K with zero point energy (ZPE) and at $T = 600$ K. Phases found to be dynamically unstable are marked with asterisks; in cases with negligible contribution of imaginary modes to the phonon density of states, we provided estimates of the distances to the convex hull with ZPE and at $T = 600$ K as well.
[a]Since Jay et al.'s study [4] did not explicitly specify the particular distribution of atoms on partial occupancy sites in each block, we considered several possible decorations and used aP414-$B_{10.5}C$ as OPO1 and mS92-$B_{6.67}C$ as OPO2.
[b]Structure from Ref. [8] after our full DFT relaxation.

Parameter	DFT	Experiment	Description	Reference
m		13.88 au	mass of 2 Li atoms	
a	2.73863 Å	2.672 Å	bond length	[10]
ν	333.01 cm^{-1}	351.43 cm^{-1}	oscillation frequency	[10]
D_0^{mol}	0.464 eV/atom	0.53 eV/atom	dissociation energy	[11]
D_0^{bcc}	1.595 eV/atom	1.63 eV/atom	cohesive energy	[11]
$D_0^{bcc\text{-}mol}$	1.131 eV/atom	1.10 eV/atom	D_0^{bcc} - D_0^{mol}	

Table S2. Parameters obtained in our density functional theory (DFT) calculations for evaluation of the chemical potential of Li diatomic gas. The corresponding experimental values are given for reference.

The chemical potential of Li_2 molecular vapor within the ideal diatomic gas model can be found as [9]

$$\mu^{\rm mol}(T,P) = E^{\rm mol} + E^{\rm mol}_{\rm ZPE} + \Delta\mu^{\rm mol}(T,P) \tag{1}$$

where the zero-point energy (ZPE) is $E^{\rm mol}_{\rm ZPE} = h\nu/2$ and the (T,P)-dependent entropy contribution is

$$\Delta\mu^{\rm mol}(T,P) = -kT\left\{ \ln\left[\left(\frac{2\pi mkT}{h^2}\right)^{\frac{3}{2}}\frac{kT}{P}\right] + \ln\left[\frac{8\pi^2 IkT}{2h^2}\right] - \ln\left[1-\exp\left(-\frac{h\nu}{kT}\right)\right]\right\}. \tag{2}$$

The $\Delta\mu^{\rm mol}(T,P)$ term combines the translational, rotational, and vibrational entropy contributions and was evaluated using the DFT parameters listed in Table S1. At 1800 K and 1 bar, these degrees of freedom contributed 78%, 27%, and 5%, respectively. Note that for comparison with experiment we used $D_0^{\rm mol} = E^{\rm mol} + E^{\rm mol}_{\rm ZPE} - E^{\rm at}$. The following expression is used to calculate the moment of inertia in the above formula: $I = 2m(a/2)^2 = ma^2/2$.

The chemical potential of bcc-Li is found within the harmonic approximation using the DFT phonon density of states $g(\omega)$ as

$$\begin{aligned}
\mu^{\rm bcc}(T,P) &= E^{\rm bcc} + E^{\rm bcc}_{\rm ZPE} + \Delta\mu^{\rm bcc}(T), \\
E^{\rm bcc}_{\rm ZPE} + \Delta\mu^{\rm bcc}(T) &= \int_0^\infty d\omega g(\omega)\frac{\hbar\omega}{2} + kT\int_0^\infty d\omega g(\omega)\ln\left[1-\exp\left(-\frac{\hbar\omega}{kT}\right)\right] \\
&= kT\int_0^\infty d\omega g(\omega)\ln\left[2\sinh\left(\frac{h\omega}{2kT}\right)\right].
\end{aligned}$$

We relied on the same expressions to map out the (T,P) phase boundaries for delithiation of LiBC. After calculating the phonon densities of states for LiBC and Li_xBC, we determined $P(T)$ for a set of temperatures by equilibrating the chemical potentials of Li in LiBC and the combination of Li_2 and Li_xBC:

$$\frac{1}{1-x}{\rm LiBC} = \frac{1}{2}{\rm Li_2} + \frac{1}{1-x}{\rm Li}_x{\rm BC}.$$

[1] T. C. King, P. D. Matthews, H. Glass, J. A. Cormack, J. P. Holgado, M. Leskes, J. M. Griffin, O. A. Scherman, P. D. Barker, C. P. Grey, S. E. Dutton, R. M. Lambert, G. Tustin, A. Alavi, and D. S. Wright, Angewandte Chemie **127**, 6017 (2015).
[2] Z. Li, C. Lu, Z. Xia, Y. Zhou, and Z. Luo, Carbon **45**, 1686 (2007).
[3] V. Milashius, V. Pavlyuk, G. Dmytriv, and H. Ehrenberg, Inorganic Chemistry Frontiers. **5**, 853 (2018).
[4] A. Jay, O. Hardouin Duparc, J. Sjakste, and N. Vast, Journal of Applied Physics **125**, 185902 (2019).
[5] A. Ueno, T. Fujita, M. Matsue, H. Yanagisawa, C. Oshima, F. Patthey, H.-C. Ploigt, W.-D. Schneider, and S. Otani, Surface Science **600**, 3518 (2006).
[6] H. Liu, Q. Li, L. Zhu, and Y. Ma, Physics Letters A **375**, 771 (2011).
[7] M. Zhang, H. Liu, Q. Li, B. Gao, Y. Wang, H. Li, C. Chen, and Y. Ma, Physical review letters **114**, 015502 (2015).
[8] V. Pavlyuk, V. Milashys, G. Dmytriv, and H. Ehrenberg, Acta Crystallographica Section C **71**, 39 (2015).
[9] P. C. Ellgen, Thermodynamics and chemical equilibrium (2014).
[10] A. I. Boldyrev, J. Simons, and P. v. R. Schleyer, The Journal of chemical physics **99**, 8793 (1993).
[11] E. Joseph and M. Haque, Asian Journal of Physical and Chemical Sciences **1**, 1 (2016).